

MEMS Inertial on an RTK GPS Receiver: Integration Options and Test Results

Tom Ford, Jason Hamilton and Mike Bobye of NovAtel Inc
John R. Morrison and Brian Kolak of Honeywell Commercial Aviation Products

BIOGRAPHIES

Tom Ford is a GPS specialist at NovAtel Inc.. He has a BMath degree from the University of Waterloo (1975) and a BSc in survey science from the University of Toronto (1981). He became involved with inertial and GPS technologies at Sheltech and Nortech surveys in 1981. He is a member of the original group of GPS receiver developers at NovAtel Inc., where he has helped develop many of the core tracking, positioning and attitude determination technologies used there. His current focus is the integration of GPS with other supplementary systems, especially INS.

Jason Hamilton has been a geomatics EIT at NovAtel Inc. since he graduated with a BSc in Geomatics Engineering from the University of Calgary in 1998. He has worked in the test and OEM development group until 2001, when he became a member of the research team at NovAtel Inc. He is focusing his efforts on GPS/INS integration and the use of phase measurements to enhance the GPS position.

Mike Bobye is a Geomatics EIT at NovAtel Inc. He started work in the customer support group and is currently a member of the GPS research group at NovAtel Inc. He graduated with a BSc in Geomatics Engineering from the University of Calgary in 1999.

Mr. Brian C. Kolak is a Principal System Engineer at Honeywell and has 16 years of experience on system definition, integration, reliability, and test, in military and commercial aviation. His experience ranges from sensors and test equipment to inertial systems, from high-end ring laser gyros (RLG) to MEMS. He also worked 2 years at ADC Telecommunications. He holds a BS in electrical engineering from Michigan Technological University.

Mr. John R. Morrison is a System Staff Engineer at Honeywell and has 19 years of experience in military and commercial aviation. He has developed inertial systems extending from high-end RLG navigators for air transport

to the current MEMS navigators for a variety of aerospace and non-aerospace markets. He holds a BS in electrical engineering from the University of Minnesota.

ABSTRACT

Inertial technology has evolved over the last fifty years from one based on iron gyros, with error control from zero velocity updates and star trackers to ring laser and fiberoptic gyros updated with GPS observations of various types. Today, micro electromechanical system (MEMS) inertial measurement units (IMU) are maturing to the state that low-cost commercialization is becoming feasible. At the same time, computer processor power is sufficient to allow both GPS and inertial data to be processed in a single processor. NovAtel Inc. and Honeywell have collaborated on the integration of the Honeywell HG1900 MEMS IMU and the NovAtel Inc. OEM4 GPS receiver. MEMS inertial and GPS data are collected and processed on the OEM4 resulting in a combined position, velocity and attitude solution that benefits from the synergies of the two technologies. The MEMS inertial navigation system (INS) provides continuous position when GPS satellite signals are not available, and reduces the time to obtain a real-time kinematic (RTK) position once GPS signals return.

The objective of the integration is to provide continuous sub-meter level positioning (2 sigma) to address future requirements of the automotive industry. The system integration is described, particularly, the major components, the timing synchronization and the filtering methodology. In order to deal with some of the error characteristics of the MEMS system, various filtering methods were investigated before the requirements were met. In addition, various GPS observables were integrated in the filter, and the impact of various types of observables was tested. Test results are presented. In particular, a filter modification incorporating current and previous states was implemented, and the effect of adding GPS delta phase measurements to this implementation was

quantified. The advantage of adding delta phase measurements is that the filter can take advantage of the low noise and small error growth of the phase measurement without the additional burden of maintaining ambiguity states. Finally, simulations were done to evaluate possible system performance improvements using distance measurement indicator (DMI) aiding.

INTRODUCTION

GPS technology has created many possibilities for new navigation applications. In the automotive market, it has already proven itself as an assistant to drivers trying to navigate their way through unknown territory. For navigation, it only needed to determine position close enough to know what road the vehicle was on; however, as GPS accuracy improves, new possibilities emerge. If the “exact” position of the vehicle could be known, then many new safety and control applications would be possible.

GPS technology has limitations, however, especially in automotive applications where the line of sight to the GPS satellites can be obscured by overpasses, signs, other vehicles, and buildings.

Inertial technology provides a solution to GPS unavailability. Inertial systems make use of gyro and accelerometer sensors to measure motion and compute position. They are self-contained and independent from GPS and are therefore unaffected by satellite blockages and signal interference.

Inertial systems have been in use for over 50 years; however, their cost has put them out of bounds for automotive applications until now, with the introduction of MEMS-based inertial systems.

In order to achieve a sub-meter performance in a low-cost system, several things are needed, including:

1. A high-quality GPS receiver
2. A source of local differential corrections to the GPS
3. A set of moderate performance and low-cost inertial sensors
4. A variety of specialized algorithms.

In this paper, we have described a specific set of these four items and the test results obtained in several vehicle scenarios.

SYSTEM DESCRIPTION

A photograph of the hardware used for this paper is shown in Figure 1. This is an early prototype of a system that could meet the requirements of the automotive industry, as

well as many other applications. It is referred to as the Integrated Positioning System (IPS).

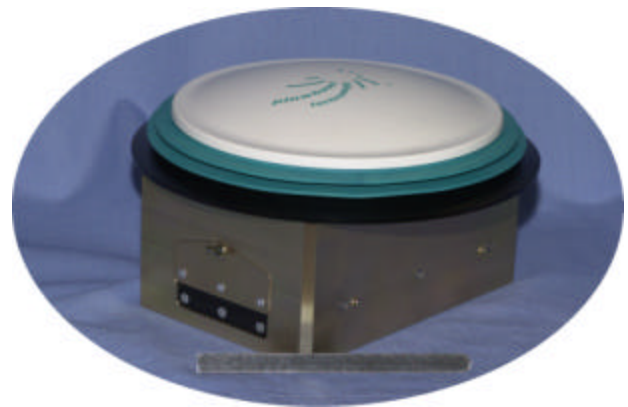


Figure 1: Integrate d Positioning System

The IPS is comprised of the following:

- GPS Antenna
- GPS Receiver
- Inertial Measurement Unit (IMU)
- Data Recorder
- Fusion Processor & Software

The system is housed in a metal chassis that can be mounted to a vehicle. The antenna is covered with a protective plastic dome. There is a connector on the bottom and an access door to the flash memory card on the side.

A block diagram of the system is shown in Figure 2.

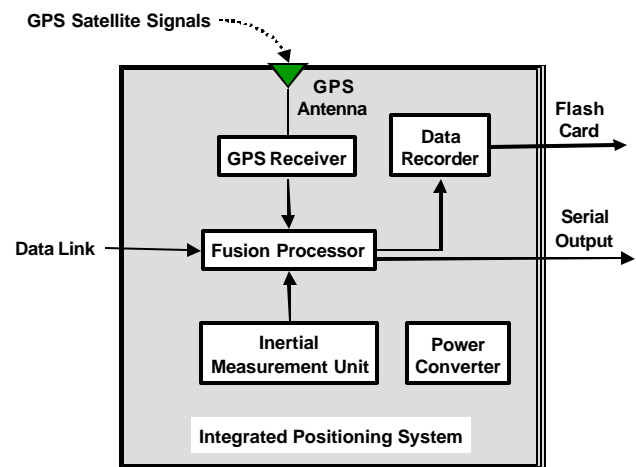


Figure 2: IPS Block Diagram

GPS RECEIVER/ANTENNA

The GPS receiver in the IPS is a NovAtel OEM-4. It features:

- 24 channels
- Dual frequency L1/L2 reception
- Multipath mitigation [8][9]
- Accepts Code and carrier differential messages
- Float and fixed ambiguity Carrier solution
- Inertial navigation algorithms and Kalman filter
- Fast reacquisition

The OEM-4 hosts the fusion processor, where all of the GPS/INS software is located. The software functionality is described in more detail in the algorithm section.

The GPS antenna is a NovAtel 600 L1/L2 antenna. It features multi-path rejection, survey quality and dual frequency capability.

MEMS IMU

Inertial Measurement Unit in the IPS is an early version of the Honeywell HG1900 MEMS IMU.



Figure 3: HG1900 MEMS IMU

The HG1900 MEMS IMU offers both cost and technical advantages.

The Honeywell IMU offers a path to low cost through high-volume production and MEMS technology. Although this unit is an early prototype, Honeywell has already pioneered high-volume production of both MEMS devices and IMUs. Honeywell's MEMS capability derives synergy from more than 25 years of experience with MEMS-based products. Taking advantage of its domain knowledge and production facilities, which

produce the world's most accomplished ring laser gyros, Honeywell ushers in the era of MEMS inertial guidance.

The MEMS sensors take advantage of the inherent low costs associated with silicon wafer fabrication techniques while providing sensitivity and ruggedness suitable for automotive use. The single-crystal silicon gyro is fabricated using a dissolved wafer process with dry etch and boron diffusion process steps utilized to define the final structure. This structure is then anodically bonded to a glass substrate that has been prepared with metallic structures that become an integral part of the rate sensor operation. The entire manufacturing process is a single micro-machined bulk process that uses only four masks.

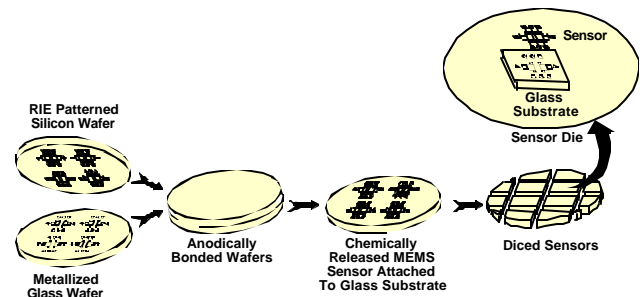


Figure 4: MEMS Silicon Process

This early version of the MEMS IMU was assembled manually and then calibrated and tested on automated high-volume equipment. Future advancements in the MEMS sensors will allow the entire IMU to be assembled automatically, much like a circuit card.

IMU TECHNICAL FEATURES

- Volume < 16 cu. in.
- Weight < 1.0 lbs.
- Power < 3 Watts
- Operating Temperature -55° to 85° C
- Full six degree-of-freedom (6-DOF) measurement system (3 gyros and 3 accelerometers)
- Honeywell silicon MEMS gyros
- Honeywell quartz resonant-beam accelerometers
- Outputs compensated for temperature and other effects

SENSOR THEORY OF OPERATION

The MEMS gyro measures rotational rate using the principle of coriolis acceleration ($A_c = w \times V$). An internal silicon mechanism is driven to a velocity V and then measures the acceleration that results from the device being rotated with a rotation w .

The quartz resonant-beam accelerometer measures linear acceleration through the use of Newton's 2nd law ($F = mA$). The device measures the force exerted on a proof mass by acceleration.

IMU PERFORMANCE CHARACTERISTICS

The inertial performance (position, velocity, attitude, etc) of the IPS unit is directly related to the performance characteristics of the IMU sensors. For reference, we have included the breakdown of sensor performance characteristics in Table 1.

Table 1: IMU Performance Characteristics

Characteristic	1s value
Output Data Rate	100 Hz
Gyro Rate Scale Factor	150 ppm
Gyro Rate Bias	
- Turn-on to turn-on	30 deg/hr
- In-run stability	10 deg/hr
Gyro Angular Random Walk	0.1 deg/root-hr
Accelerometer Scale Factor Accuracy	300 ppm
Accelerometer Linearity	500 ppm
Accelerometer Bias	1 mg

IMU performance is expected to improve over time. How far beyond the performance of this early version of the MEMS IMU is yet to be determined.

DATA RECORDER

The data recorder in the IPS unit is a NovAtel PDCard. It stores output data messages in real time for later post-processing and analysis. Its data collection medium is a compact flash card interfaced to a serial link that transfers data at 230k baud.

OTHER EQUIPMENT

In addition to the IPS unit, other equipment was used for testing. Figure 5 depicts the relationship of the other equipment to the IPS.

There is a stationary ground-based segment consisting of a GPS base station and a data link base. The base station obtains local differential GPS (DGPS) corrections and broadcasts them via the link.

There is a moving vehicle segment consisting of a data link rover, the IPS, and PC-based monitoring equipment. The data link rover picks up the DGPS correction broadcasts and sends them to the IPS via a serial interface.

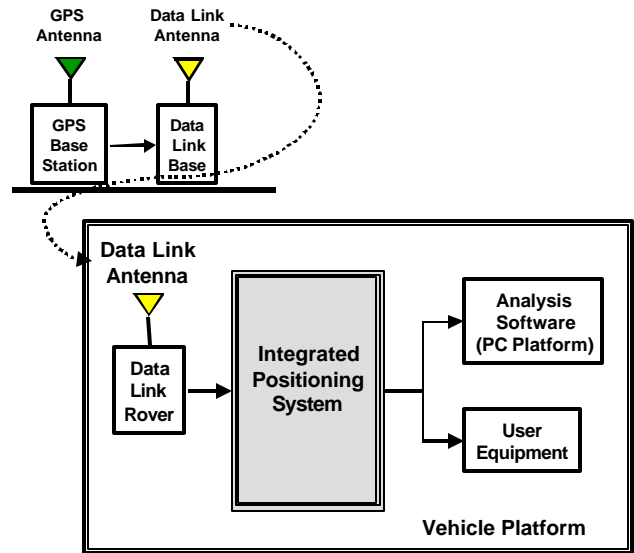


Figure 5: Interfacing Equipment

GPS BASE STATION

The GPS base station consists of a NovAtel OEM4 GPS receiver, model 600 L1/L2 GPS antenna, and PDCard data recorder. The base station mounts on a tripod.

Although it is capable of many formats, the base station was configured to receive, record, and transmit RTCA type 1 differential corrections. Range and phase data are transmitted via serial interface to the data link for real time processing. Range, phase, ephemeris and almanac data are recorded in the data recorder for post processing.

DATA LINK

The data link is a Pacific Crest Corporation Positioning Data Link™ (PDL™) with the following features:

- 2 or 35 Watts
- 450 – 470 MHz
- 38,400 baud.

POSITIONING FILTER ALGORITHMS

The IPS software contains the algorithms to compute a high-accuracy integrated GPS/INS solution. The solution takes advantage of the fast update rates and independence of the inertial system and the high accuracy of the GPS in an optimal integrated solution.

INTEGRATION SOFTWARE ARCHITECTURE

The OEM4 software consists of numerous tasks, including tracking, GPS observation generation, pseudorange filtering, RTK ambiguity resolution, low latency RTK position generation, low latency inertial system maintenance and inertial error control. A high-level view of the system software architecture is shown in Figure 6.

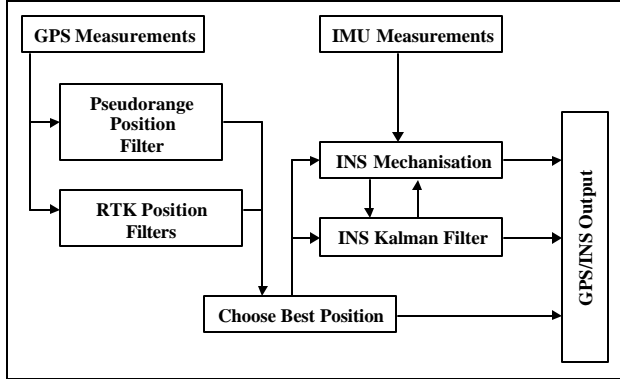


Figure 6: OEM4 Positioning Tasks

Inertial solution errors are damped principally by GPS position updates, be they pseudorange single point positions, differential pseudorange positions or RTK positions based either on floating or fixed ambiguity estimates. These are supplemented by zero velocity updates (ZUPTS) and in some cases, delta phase updates.

The IMU measurements are provided to the IMU task at a 100 Hz rate and include three specific force measurements and three delta angles per sample. The delta angles are reduced by the known earth rate and estimated gyro bias measurements before being used to update the system attitude, which is maintained as a quaternion vector. The specific force measurements are adjusted for the modeled gravity vector, for the velocity dependent coriolis force, and estimated accelerometer biases before being integrated once to generate velocity and again to generate position.

KALMAN FILTER DESIGN

The inertial system error modeling includes either 15 or 21 Kalman filter error states. The basic 15-state model, described in [2] and [3] and used for the real-time system, includes 3 states for each of position, velocity and attitude, all in the Earth Centered Earth Fixed (ECEF) frame. In addition, the filter includes 6 states for accelerometer and gyro time-dependent biases. The bias states are axis specific and are parameterized in the body frame of the IMU. In the 21-state filter, used in the post mission system, three additional states are included for IMU to GPS antenna offset estimation, and three more states are included to represent position errors at the last update time. Thus, current and previous positions can be directly linked with measurements such as phase difference or wheel pick off outputs. It is worthwhile to examine

Kalman filter design in more detail in the 21-state case. At the outset, there was speculation that comparisons to a system in which scaling error estimation was incorporated would be included, but the scaling error on the HG1900 is relatively small, so this analysis was not included. Test results presented here have been generated from the 21-state filter.

The general form of the Kalman filter propagation and update equations [1] are described by the following equations:

Propagation:

$$\text{State: } x(-) = \Phi x(+)$$

$$\text{Covariance } P(-) = \Phi P(+)\Phi^T + Q$$

where x is the state vector (+) after update, (-) after propagation

P is the state variance covariance matrix

Φ is the transition matrix, the time solution of the dynamics matrix describing the dynamics of the system

Q is the matrix describing the time propagation of the spectral densities of the state elements.

Update step:

$$K = P(-)H^T(HP(-)H^T + R)^{-1}$$

$$x(+) = x(-) + K(z - Hx(-))$$

$$P(+) = (I - KH)P(-)$$

where z is the observation vector

R is the observation variance covariance matrix

H is the linear relationship between the observation and state vector

K is the Kalman gain matrix

In the Kalman framework, the method used to incorporate observations that span the time interval between successive epochs was to explicitly include previous position states in the state vector. For example, the state vector for the 21-state model in expanded form is

$$dx = \begin{bmatrix} dr_t^e & dv^e & e^e & db^b & b^b & o^b & dr_{t-1}^e \end{bmatrix}^T$$

All the entries noted in the state vector represent three element vectors of, in the order listed, current position error, velocity error, attitude error (all in the ECEF frame), gyro and accelerometer biases (in the body frame) and finally, in the 21-state case, antenna offset and previous position error.

The Kalman propagation step

$$P(-) = \Phi P(+)\Phi^T + Q$$

of the covariance is done once per ½ second. Post update feedback of the state to the system makes state propagation unnecessary.

The initial P matrix elements are assigned based on the best knowledge available after the system alignment. This is a function of the system parameters, the type of GPS position available and the quality of the alignment, including the time in stationary mode and on the noise level of the IMU measurements used in the alignment. The horizontal components of the attitude can be estimated to an accuracy dictated by the level of accelerometer bias, or about 0.06 degrees. A large variance (200 degrees squared) is assigned to the heading element of the covariance matrix after the coarse alignment. The heading is only refined once the system begins to move.

OBSERVABLES

The system is capable of using positions, zero velocities, phase differences or along track position differences as inputs. The H matrices associated with the various update types are as follows:

Position:

$$H = \begin{bmatrix} I & 0 & 0 & 0 & 0 & 0 & 0 \end{bmatrix}$$

Velocity:

$$H = \begin{bmatrix} 0 & I & 0 & 0 & 0 & 0 & 0 \end{bmatrix}$$

Where I is a 3-by-3 identity matrix and 0s are 3-by-3 zero matrices

Delta phase:

This is described more fully in a GPS-only application [4], but the basic equations are repeated here for convenience. The double difference phase across time and satellites (reduced by satellite motion and atmospheric effects) can be modelled as:

$$\nabla\Delta\phi_{112}^{ij} = \nabla H^{ij} (x_{t2} - x_{t1})$$

Where ∇H^{ij} is the vector

$$\nabla H^{ij} = [\Delta x^i/R^i - \Delta x^j/R^j, \Delta y^i/R^i - \Delta y^j/R^j, \Delta z^i/R^i - \Delta z^j/R^j]$$

Where Δx^i (etc) is the difference between the x components of the GPS antenna position and the position of the i^{th} satellite, and R^i is the distance between the antenna and the i^{th} satellite. The “H” used in the gain calculation is:

$$H^{ij} = [\Delta x^i/R^i - \Delta x^j/R^j, \Delta y^i/R^i - \Delta y^j/R^j, \Delta z^i/R^i - \Delta z^j/R^j, \\ 0,0,0, 0,0,0, 0,0,0, 0,0,0, 0,0,0, \\ -\Delta x^i/R^i + \Delta x^j/R^j, -\Delta y^i/R^i + \Delta y^j/R^j, -\Delta z^i/R^i + \Delta z^j/R^j]$$

The along track position difference observable is quite similar in formulation to the delta phase observable, so the details of this formulation are omitted.

MISCELLANEOUS SYSTEM ELEMENTS

This section describes a number of system subtasks that are important to the current and future operation of the system, but are not central to the performance metrics described in this paper. Included in this section are descriptions of the time synchronization of the IMU measurements with GPS time, the alignment methodology, and the RTK process in the presence of inertial data. Included with the alignment portion of the description is a note on the system’s operation at startup in the absence of GPS measurements.

The foundation of the RTK portion of this system is the NovAtel Inc. RTK process, which has been under development since 1994 [5][6]. Ambiguities are estimated via a two-step process. In the first, a floating ambiguity estimate is computed and refined over time. Once the accuracy of the floating ambiguity reaches a certain level, the associated position and uncertainty is used to define a search space about which possible ambiguity candidates are selected and eliminated over time depending on the accumulated residual history each candidate generates. In the IPS unit, short GPS outages are bridged via a single initialization per resolution of the floating ambiguity filter with the position maintained by the INS. This is described more fully in [3] with regards to a previous GPS/INS integration.

When each HG1900 IMU record is generated, the IMU coincidentally generates a pulse. This pulse triggers the OEM4 to capture GPS time. Then the IMU message is assembled by the OEM4 and time tagged with the previously generated system time. The total time tagging error is less than 1 millisecond.

The alignment of the system is described in [2][7]. The general principle used in the alignment is that the gravity vector projects onto the horizontal accelerometers, and this relationship is used to determine horizontal attitude to an accuracy that is dependent on noise and accelerometer bias. In this case, the initial horizontal attitude is accurate to 0.06 degrees. At the same time, the earth rate vector projects onto the rate gyro, and this is used to determine heading. The gyro bias level limits the accuracy of the stationary heading portion of the alignment, and the heading does not become observable in this process. To compute heading, horizontal acceleration is required, and steady state heading accuracy is not reached until the system has been moving for approximately 100 seconds. This alignment time can be reduced somewhat by using an injected heading based upon GPS velocity, but in this case, the angular offset between the body frame of the

IMU and the vehicle frame must be known, and the vehicle movement must be aligned with the vehicle body frame.

During normal steady state operation, the IPS software senses when it is stationary, and during these interludes, stores its various system elements (position, assumed zero velocity, attitude, biases etc.). With the assumption that the system only moves when it is powered, it can use the previously stored system information to rapidly initialize all of the states at power-up.

PERFORMANCE GOALS AND VALIDATION

The objective of this exercise was to integrate the Honeywell HG1900 MEMS IMU with a NovAtel Inc. OEM4 dual frequency GPS receiver and to evaluate the integrated system performance in various environments. We aimed at achieving an informal benchmark of 10cm position accuracy after a 10-second GPS outage, provided the GPS receiver had been operating in RTK mode prior to the outage. Secondary to this benchmark is an attitude accuracy of 0.015 degrees (pitch and roll), and 0.05 degrees (heading). Using the performance characteristics as defined in Table 1, the performance expectation for the system was calculated to be approximately 50cm position error (1 sigma) after a 10-second GPS outage. The expectation for attitude accuracy was 0.05 degrees in roll and pitch and better than 0.2 degrees in heading. The basic performance of the system was benchmarked with updates being restricted to GPS positions only. Various additional observables beyond GPS position and zero velocity updates, such as delta phase measurements and delta position differences (ie wheel pickoffs) are or may become available, so the system performance with and without those elements is quantified.

TEST SETUP

The equipment was tested in a van. The IPS unit was located on a rack on top of the van. The rover data link antenna was located next to the IPS unit. The remainder of the vehicle equipment was located inside the van. The base station was set up near the center of the course in the middle of an open field with a full view of the sky. The farthest point from vehicle to base station was about 600 meters. A high-quality Inertial Reference System (IRS) was used as a control or truth system for attitude comparison to the IPS unit. This control system was a Honeywell HG2100 ring-laser-gyro-based IRS with typical attitude performance of 0.1 deg/hr at the 2-sigma level.

TEST ROUTE

In order to quantify the system performance, a course was designed to test the repeatability of the system under

controlled conditions. Part of the design criteria was good satellite visibility so that centimeter level control position accuracy was available all the time. A secondary criteria was that the same route should be followed repeatedly, so the system performance under the same conditions could be evaluated repeatedly. Although various test scenarios took place during the development, this particular test was chosen to demonstrate the system capabilities because it satisfied the continuity and repeatability criteria, and a high-accuracy inertial system was available during that test. The route selected was a rectangular block with approximately 1 km per side, and the block was traversed 8 times over a time interval of 2400 seconds. This route is shown in Figure 7, below.

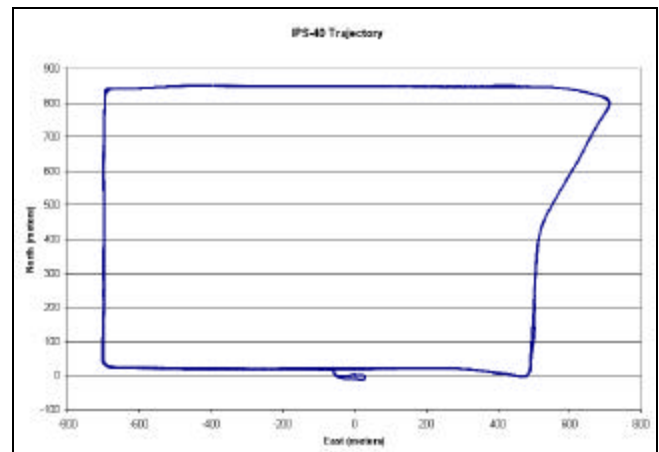


Figure 7: Test Route

RESULTS

Attitude accuracy was determined by comparing the IPS attitude output to the IRS. There is some jitter on the angular differences, and part of this is a result of the small (sub 10 msec) differences in time synchronization between the two units. In addition, there were constant offsets between the three axis of the two systems, but the size of the variation in the agreement can give a good estimate of the total error of the IPS unit. The two INS systems are not absolutely time synchronized, and there is some evidence of variation in the measurement of time on the HG2100 compared to the IPS unit, which is synchronized with GPS to the millisecond level. A $\frac{1}{2}$ degree error during times when the system is turning can be caused by a timing error between the two inertial systems of 0.025 seconds, and this level of timing error is not out of the question. In spite of this, the two systems gave fairly consistent attitude outputs, and the reported standard deviation for the IPS attitude was reasonably consistent with the discrepancies. The standard deviation of the steady state attitude differences and the average reported standard deviations from the system are shown in Table 2. The standard deviation of the differences are in the row "Computed Stdev." The "Reported Stdev" in the table represents the

root mean square of the system's reported standard deviations based on the 2500 seconds worth of data in the test. Given the uncertainty of the time synchronization and the noise on the control system, the reported uncertainty agrees quite well with the nominal discrepancy.

Table 2: Steady State Attitude Errors

	Pitch Diff	Roll Diff	Heading Diff
Computed Stdev	0.054 deg	0.047 deg	0.28 deg
Reported Stdev	0.04 deg	0.04 deg	0.16 deg

The system reaches steady state in normal mode (without any previous alignment knowledge) after approximately 120 seconds. If there is previous knowledge, steady state is achieved sooner.

Position accuracy was determined by comparing the system INS position output to the positions determined from GPS operating in RTK mode. Steady state agreement is, as expected, very good, so error growth over time in the absence of GPS is measured by comparing the INS positions without GPS to RTK GPS position for short (10 second and 20 second) time intervals. In order to see how the system reacts under varying conditions of restricted satellite availability, different observation scenarios were devised to illustrate these conditions. There were seven different observation scenarios, as described in the following list (the bracketed short forms appear as descriptors for the various tests in the figures 8 to 11 and in tables 3 to 6):

1. No updates at all (No Update)
2. A simulated wheel pick off (Whl)
3. One delta phase measurement (1 DP)
4. Two delta phase measurements (2 DP)
5. Three delta phase measurements (3 DP)
6. Simulated wheel pick off in combination with one delta phase measurement (1DP + Whl)
7. Simulated wheel pick off in combination with two delta phase measurements (2DP + Whl)

The different scenarios were applied on straight and curved sections of a trajectory consisting of an approximately rectangular loop (Figure 7). The straight section outage took place on the south west traverse just south of the sharp north east curve. The curve sections took place on the north east curve. The outage time was 10 seconds, and then 20 seconds. In all cases, the outage performance tests did not start until the system had reached steady state with RTK type GPS control. The delta phase measurements were double difference measurements based on the phase provided by the remote receiver. The differences were taken across two satellites and across time. The simulated wheel pick off measurement was the distance between successive RTK

GPS measurements. There were six outage tests for each scenario.

The plots in Figures 8, 9, and 10 show typical error growth for the ensemble of outage and observation types for the north, east and up position components during the 10-second duration curved section tests. This set of plots corresponds to a particular outage interval whose performance contributes to the summary tables 4a, 4b and 4c. Figure 8 and 9 show the horizontal error growth, while Figure 10 shows the error growth in height as well as the standard deviation of the height when there are no updates and when two delta phase measurements are available. The plots show that the expected error damping associated with the supplementary measurements, as well as the correspondence between the actual error in height and the reported error.

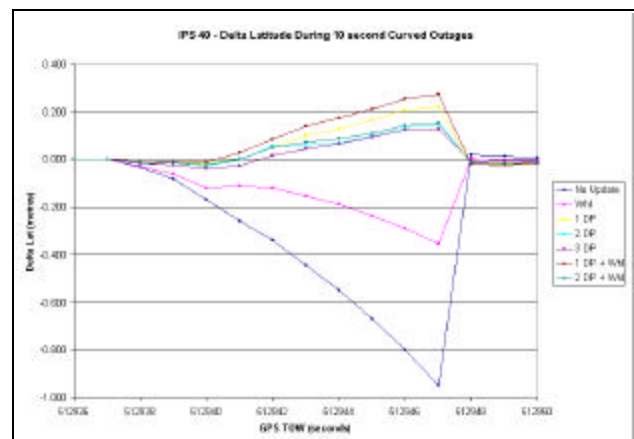


Figure 8: North Position Error with 10-second outage

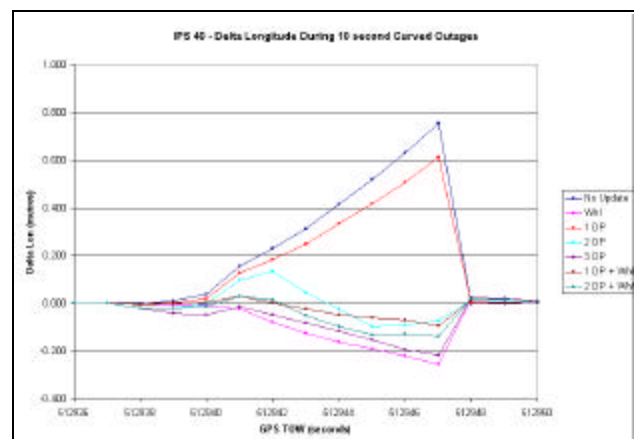


Figure 9: East Position Error with 10-second outage

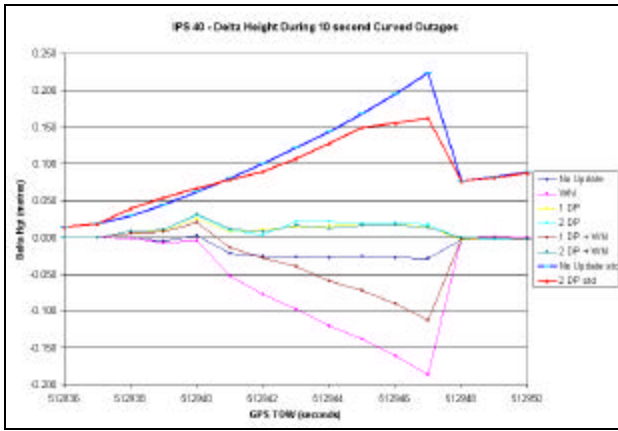


Figure 10: Height Position Error with 10-second outage

It is worthwhile to include an additional Figure 11, which demonstrates the reported error growth in a horizontal direction (north) and the correspondence it has to the growth in north error.

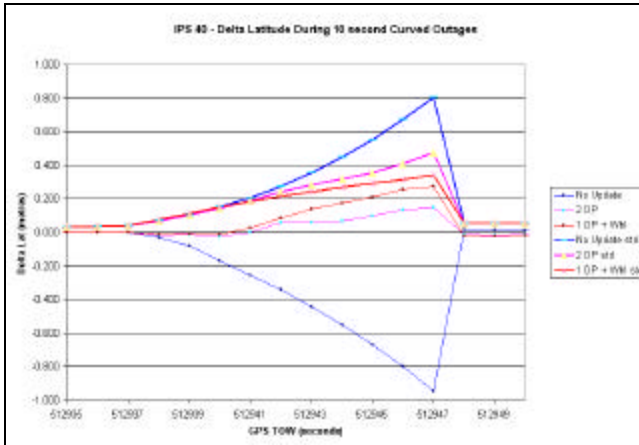


Figure 11: North Position Errors and Standard deviations with 10-second outage

This shows a typical correspondence between the size of the actual error and the reported magnitude of the error. This and other similar plots demonstrate that the system truthfully represents the errors in the system.

The final position error and reported standard deviation for each of the 10-second outages was determined, and then an RMS and maximum value was computed across all of the outages. These values are tabulated in the columns of the remaining tables of this paper. The root mean square of the system position differenced from control at the end of the outage interval is given in the following tables as RMS (m). The system's reported standard deviations at the end of the outage interval indicated the system's expected error at that time. The root mean square of these standard deviations are included in the tables under RMS Std (m). This gives an indication of the reliability of the

system's knowledge of its own errors. Finally, the maximum error at the end of the intervals is included to indicate the distribution of the errors in the tests.

The summary of the system performance in the absence of GPS for 10 seconds during a straight section is shown in Tables 3a, 3b, and 3c. Whl stands for simulated Wheel Pick Off.

Table 3a: North Position Error Summary

	RMS (m)	RMS Std (m)	Max Err (m)
No Update	0.255	0.509	-0.429
Whl	0.093	0.455	0.164
1 DP	0.090	0.503	0.134
2 DP	0.041	0.424	-0.069
3 DP	0.047	0.265	-0.099
1 DP + Whl	0.088	0.421	0.123
2 DP + Whl	0.040	0.358	-0.066

Table 3b: East Position Error Summary

	RMS (m)	RMS Std (m)	Max Err (m)
No Update	0.297	0.419	-0.647
Whl	0.197	0.306	-0.315
1 DP	0.282	0.223	-0.601
2 DP	0.151	0.215	0.204
3 DP	0.049	0.206	0.076
1 DP + Whl	0.162	0.216	-0.321
2 DP + Whl	0.118	0.204	0.190

Table 3c: Height Position Error Summary

	RMS (m)	RMS Std (m)	Max Err (m)
No Update	0.162	0.128	0.255
Whl	0.160	0.132	0.255
1 DP	0.160	0.127	0.252
2 DP	0.161	0.132	0.291
3 DP	0.160	0.127	0.307
1 DP + Whl	0.148	0.136	0.249
2 DP + Whl	0.155	0.142	0.288

Tables 4a, 4b, and 4c show a summary of the system performance when the 10-second outages occur during curved sections of the trajectory.

Table 4a: North Position Error Summary

	RMS (m)	RMS Std (m)	Max Err (m)
No Update	1.116	0.393	-2.247
Whl	1.058	0.256	-2.310
1 DP	0.197	0.390	0.308
2 DP	0.098	0.314	0.185
3 DP	0.086	0.229	0.160
1 DP + Whl	0.170	0.260	0.251
2 DP + Whl	0.103	0.257	0.162

Table 4b: East Position Error Summary

	RMS (m)	RMS Std (m)	Max Err (m)
No Update	0.482	0.540	-0.952
Whl	0.358	0.483	-0.770
1 DP	0.411	0.245	-0.741
2 DP	0.190	0.218	-0.295
3 DP	0.108	0.218	-0.202
1 DP + Whl	0.088	0.244	-0.154
2 DP + Whl	0.065	0.224	-0.147

Table 4c: Height Position Error Summary

	RMS (m)	RMS Std (m)	Max Err (m)
No Update	0.133	0.156	-0.227
Whl	0.175	0.147	-0.328
1 DP	0.142	0.145	-0.215
2 DP	0.181	0.122	0.323
3 DP	0.134	0.131	0.221
1 DP + Whl	0.173	0.149	-0.239
2 DP + Whl	0.148	0.135	0.224

Some comments can be made based on the 10-second results.

1. The plots show discontinuities during the free inertial sections, which are a result of noise on the RTK control stemming from the fact that base station measurements were taken only once every 10 seconds. The discontinuities occurred when a position from a set of extrapolated base station measurement is juxtaposed with a position generated from a set of time matched base and rover measurements. The extrapolated error in control adds approximately 5 cm to the measured uncertainty.
2. The RMS error of the free inertial is at the 0.6 meter level. Over straight section outages, the horizontal error is less than 0.30 meters.
3. The best performance is in height, and the various updating aids don't seem to help significantly.
4. The delta phase measurement significantly improves the position error in north (to less than 20 cm), but to a lesser extent in east. The east improvement is not as

dramatic, and at least 2 delta phase measurements are required before the position error improves.

5. The wheel pick off significantly improves position accuracy in some, but not all, cases. This is true for a single delta phase measurement, as well. A single delta phase observation applied with the wheel pick off "measurement" restricts the horizontal error to less than 0.20 meters after 10 seconds.
6. The RMS standard deviations are included in Figure 11 to demonstrate correspondence between the system errors during the outage and the reported standard deviations. In general, the system errors are truthfully reported by the position error standard deviations.

The summary of the system performance in the absence of GPS for 20 seconds during a straight section is shown in Tables 5a, 5b, and 5c. Whl stands for simulated Wheel Pick Off.

Table 5a: North Position Error Summary

	RMS (m)	RMS Std (m)	Max Err (m)
No Update	1.038	1.741	1.655
Whl	0.281	1.491	0.383
1 DP	0.180	1.729	0.327
2 DP	0.135	0.916	0.240
3 DP	0.192	0.420	-0.357
1 DP + Whl	0.166	0.891	0.309
2 DP + Whl	0.161	0.615	-0.296

Table 5b: East Position Error Summary

	RMS (m)	RMS Std (m)	Max Err (m)
No Update	0.931	1.488	-1.925
Whl	0.698	0.858	-1.084
1 DP	0.887	0.372	-1.781
2 DP	0.775	0.350	1.156
3 DP	0.177	0.307	0.328
1 DP + Whl	0.444	0.350	-0.623
2 DP + Whl	0.276	0.306	0.509

Table 5c: Height Position Error Summary

	RMS (m)	RMS Std (m)	Max Err (m)
No Update	0.232	0.244	-0.459
Whl	0.228	0.250	-0.440
1 DP	0.223	0.237	-0.415
2 DP	0.174	0.234	-0.280
3 DP	0.185	0.200	0.291
1 DP + Whl	0.187	0.236	-0.351
2 DP + Whl	0.155	0.228	0.263

Tables 6a, 6b, and 6c below show a summary of the performance of the system if the GPS outages take place during curved sections of the trajectory for a period of 20 seconds.

Table 6a: North Position Error Summary

	RMS (m)	RMS Std (m)	Max Err (m)
No Update	2.842	1.317	-6.270
Whl	2.670	0.488	-5.835
1 DP	0.615	1.297	0.959
2 DP	0.376	0.796	0.550
3 DP	0.252	0.362	0.419
1 DP + Whl	0.553	0.454	0.805
2 DP + Whl	0.292	0.455	0.444

Table 6b: East Position Error Summary

	RMS (m)	RMS Std (m)	Max Err (m)
No Update	1.756	1.508	-3.332
Whl	0.615	1.381	-1.336
1 DP	1.343	0.453	-1.949
2 DP	0.643	0.389	1.227
3 DP	0.245	0.356	-0.345
1 DP + Whl	0.177	0.444	0.324
2 DP + Whl	0.214	0.372	0.417

Table 6c: Height Position Error Summary

	RMS (m)	RMS Std (m)	Max Err (m)
No Update	0.393	0.353	-0.652
Whl	0.424	0.333	-0.680
1 DP	0.301	0.322	-0.480
2 DP	0.252	0.223	0.490
3 DP	0.133	0.215	0.252
1 DP + Whl	0.338	0.301	-0.483
2 DP + Whl	0.145	0.226	0.294

Some comments can be made based on the 20 second results.

1. The extrapolated error in control adds approximately 5 cm to the measured uncertainty.
2. The unaided error growth in the system position was between 1.0m (straight sections) and 2.5m (curved sections) horizontally and less than 0.4 m in height.
3. The wheel pick off had a significant effect on horizontal position accuracy in some cases, improving the north error on the straight sections from 1.03 meters to 0.28 meters, and the east error on the curved sections from 1.75 meters to 0.61 meters.
4. The horizontal position error growth was restricted to the 0.5 meter level after 20 seconds when one delta phase measurement is included with the wheel pick off measurement. Updates from two delta phase measurements and the wheel pick off “measurement” resulted in restricting the error growth to less than 0.3 meters after a 20 second GPS outage.

CONCLUSIONS

Honeywell and NovAtel Inc. jointly developed an integrated navigation sensor that uses an early version of the Honeywell HG1900 MEMS IMU and the NovAtel Inc. OEM4 GPS receiver. In this paper, the IMU sensor and the methodology used to combine the IMU measurements with the GPS measurements from the OEM4 sensor are described. Test results are provided which describe some aspects of the system performance.

Preliminary performance testing has shown that the sensor provides 0.6 meter positioning accuracy during GPS outages that last 10 seconds or less, provided that RTK-type GPS positions were available to the fusion filter prior to the outage. After 20 seconds, the horizontal error is between 1.0 meter (straight sections) and 2.5 meters (curved sections). The discrepancy in performance between straight and curved sections indicates that there is likely an unidentified system error that requires further investigation.

Results in Tables 3 and 4 indicate that it is possible to reduce position errors during short (10-second) outages through the use of alternative updates. The data shows the position accuracy after 10-second outage with 1 delta phase measurement will be 0.3 meters, with 2 delta phase measurements 0.2 meters, and with 2 delta phase measurements and a wheel pick off sensor, 0.15 meters.

Results in Tables 5 and 6 indicate that it is possible to reduce position error during longer (20-second) outages through the use of alternative updates. The data shows that the position accuracy after 10-second outage with 1 delta phase measurement will be reduced in some directions, but not all. With 2 delta phase measurements, the system RMS error in the horizontal directions is at the 0.5 meter level and with 2 delta phase measurements and a wheel pick off sensor, 0.3 meters.

The vertical error is at the 0.15-meter level after 10 seconds. After 20 seconds, the position error in height is at the 0.3-meter level.

Preliminary tests show that the steady state accuracy of the attitude components of the system are 0.05 degrees for pitch and roll, and 0.2 degrees for heading.

Preliminary tests show that the statistics output by the system are a fair representation of the system position and attitude errors.

ACKNOWLEDGMENTS

The authors would like to acknowledge the efforts of Michael Jones of NovAtel Inc. for his efforts in time synchronization and Gabe Selinger of Honeywell for the time spent collecting data used in the system validation.

REFERENCES

- [1] R.G. Brown, P. Hwang, **Introduction to Random Signals and Applied Kalman Filtering 2nd Edition**, John Wiley & Sons Inc, 1983
- [2] T. Ford, J. Neumann, M. Bobye “OEM4 Inertial: An Inertial/GPS Navigation System on the OEM4 Receiver”, Presented at the International Symposium on Kinematic Systems in Geodesy, Geomatics and Navigation (KIS), Banff, Alberta, Sept. 2001
- [3] T. Ford, J. Neumann, P. Fenton, M. Bobye, J. Hamilton, “OEM4 Inertial: A Tightly Integrated Decentralised Inertial/GPS Navigation System”, Proceedings of ION GPS 2001, Salt Lake City, Utah, Sept. 12-14, 2001.
- [4] T. Ford, J. Hamilton, “NovAtel Inc. New Positioning Filter: Phase Smoothing in the Position Domain”, Proceedings of ION GPS '02, Portland, Oregon, Sept. 25-27, 2002.
- [5] Ford, T.J. and J. Neumann , NovAtel's RT20 - “A Real Time Floating Ambiguity Positioning System”, Proceedings of ION GPS '94, Salt Lake City, Utah, Sept. 20-23, 1994, The Institute of Navigation, Washington, D.C. pp. 1067.
- [6] J. Neumann, A. Manz, T. Ford, O. Mulyk, “Test Results from a New 2 cm Real Time Kinematic GPS Positioning System”, Proceedings of ION GPS '96, Kansas City, Mo., Sept. 17-20, 1996, The Institute of Navigation, Washington, D.C. pp. 183
- [7] K. Britting, Inertial Navigation Systems Analysis, John Wiley and Sons Inc 1971
- [8] A. J. Van Dierendonck, P. Fenton, T. Ford, “Theory and Performance of Narrow Correlator Spacing in a GPS Receiver”, Navigation: Journal of the Institute of Navigation, Vol 39, No. 3, Fall 1992.
- [9] B. Townsend, P. Fenton, “A Practical Approach to the Reduction of Pseudorange Multipath Errors in a L1 GPS Receiver”, Proceedings of ION GPS '94, Salt Lake City, Utah, Sept. 20-23, 1994, The Institute of Navigation, Washington, D.C.